Hydrodynamic simulations of the interaction between an AGB star and a main-sequence companion in eccentric orbits

Jan E. Staff,[1,2]★ Orsola De Marco,[1,2] Daniel Macdonald,[1,2,3] Pablo Galaviz,[1,2]
Jean-Claude Passy,[4] Roberto Iaconi[1,2] and Mordecai-Mark Mac Low[5,6]

[1]*Department of Physics and Astronomy, Macquarie University, Sydney, NSW 2109, Australia*
[2]*Astronomy, Astrophysics and Astrophotonics Research Centre, Macquarie University, Sydney, NSW 2109, Australia*
[3]*Laboratoire Lagrange, UMR7293, CNRS, Observatoire de la Côte d'Azur, Université de Nice Sophia-Antipolis, F-06304 Nice Cedex 4, France*
[4]*Argelander Institut für Astronomie, D-53121 Bonn, Germany*
[5]*Department of Astrophysics, American Museum of Natural History, New York, NY 10024, USA*
[6]*Zentrum für Astronomie der Universität Heidelberg, Institut für Theoretische Astrophysik, D-69121 Heidelberg, Germany*

ABSTRACT

The Rotten Egg Nebula has at its core a binary composed of a Mira star and an A-type companion at a separation >10 au. It has been hypothesized to have formed by strong binary interactions between the Mira and a companion in an eccentric orbit during periastron passage ∼800 yr ago. We have performed hydrodynamic simulations of an asymptotic giant branch (AGB) star interacting with companions with a range of masses in orbits with a range of initial eccentricities and periastron separations. For reasonable values of the eccentricity, we find that Roche lobe overflow can take place only if the periods are ≪100 yr. Moreover, mass transfer causes the system to enter a common envelope phase within several orbits. Since the central star of the Rotten Egg nebula is an AGB star, we conclude that such a common envelope phase must have lead to a merger, so the observed companion must have been a tertiary companion of a binary that merged at the time of nebula ejection. Based on the mass and time-scale of the simulated disc formed around the companion before the common envelope phase, we analytically estimate the properties of jets that could be launched. Allowing for super-Eddington accretion rates, we find that jets similar to those observed are plausible, provided that the putative lost companion was relatively massive.

Key words: hydrodynamics – methods: numerical – binaries: close – stars: evolution.

1 INTRODUCTION

OH 231.8+4.2 is a binary consisting of an asymptotic giant branch (AGB) star with a progenitor zero-age main-sequence mass of ∼3 $M_\odot$ (found from cluster membership; Jura & Morris 1985) orbited by a companion that is most likely a less massive A0V main-sequence star (with a mass of 1.5–2.5 $M_\odot$; Sánchez Contreras, Gil De Paz & Sahai 2004). The orbital separation is poorly constrained. Sánchez Contreras et al. (2004) assumed the binary separation to be 50 au due to the presence of SiO, OH and H_2O maser emission. Schwarz et al. (1995) argued that it must exceed 10 au, or else the observed maser would be tidally disrupted. Surrounding the binary is a thick torus of gas and dust, while two highly collimated lobes extend perpendicular to the torus. The kinematic age of the lobes indicates that they were formed ∼800 yr ago (Bujarrabal et al. 2002). Both the torus and lobes contain approximately half a solar mass of dust and gas. The energy and linear momentum contained in the collimated outflows was measured to be 3 × 10^{46} erg and 3 × 10^{49} g cm s^{-1}, respectively (Alcolea et al. 2001; Bujarrabal et al. 2002). One lobe is longer than the other and appears to be breaking out of a bubble structure. The nebula has been nicknamed the Rotten Egg and Calabash nebula.

Soker & Kashi (2012) suggested that the Rotten Egg Nebula, as well as other nebulae with similar characteristics of collimated, high-momentum ejecta (e.g. IRAS22036+5306), were formed by the interaction of the two stars in the binary during periastron passage. During the short-lived interaction time, mass would accrete from the AGB star to the main-sequence companion and an accretion disc would form. This disc could launch jets that interact with the circumstellar environment leading to the inflation of lobes. They also proposed that such an interaction could repeat every periastron passage or every time a periastron passage coincides with an instability of the giant, such as a thermal pulse in the case of an AGB star. Kashi & Soker (2010) additionally suggested that the gravitational potential of the companion during periastron may be the actual

★ E-mail: jstaff@ufl.edu

trigger of such an outburst on the primary. Interactions such as these have been suggested to explain light outbursts such as Intermediate Luminosity Optical Transients (ILOTs; Kashi, Frankowski & Soker 2010, also known as Intermediate Luminosity Red Transients or Red Novae) in isolation or preceding more dramatic interactions such as common envelope (CE), leading to compact binaries or mergers.

It may be argued that giant stars should never be found in binaries with eccentric orbits, because tidal circularization time-scales are relatively rapid ($\lesssim 1000$ yr; Soker 2000). However, eccentric binaries with relatively small orbital separations do exist. A high 10 per cent of the sequence E stars in the Large Magellanic Cloud (LMC) are such binaries (Nicholls & Wood 2012). These stars are ellipsoidal variables where a red giant branch (RGB) or an AGB star is in a close orbit with a main sequence companion and the eccentricity has been observed to be as high as ~0.4 (Nicholls & Wood 2012). Soker (2000) suggested that enhanced mass-loss rate during periastron passages could increase the eccentricity, explaining why such eccentric systems exist.

Here, we carry out the first study of the viability of the proposal that binaries in eccentric orbits could interact strongly enough to promote the repeated ejection of relatively massive collimated structures. Accretion of mass on to the companion from the *wind* of an AGB star has been studied and deemed unlikely to drive the massive jets observed in nebulae like the Rotten Egg Nebula (Huarte-Espinosa et al. 2013). We therefore carry out hydrodynamic simulations of the accretion of mass on to a companion during Roche lobe overflow (RLOF). Since we need an RLOF event to take place at periastron, we exclude any orbit with a period $\gg 100$ yr, since otherwise the eccentricity would have to approach unity to allow a periastron separation sufficiently short for an RLOF to occur.

Hydrodynamical simulations of interacting binaries are challenging, particularly for eccentric orbits. A few groups have simulated similar setups using a variety of techniques. Church et al. (2009) used an 'oil-on-water' smoothed particle hydrodynamics (SPH) technique to simulate binaries consisting of a white dwarf and a main-sequence star with a range of eccentricities to measure the semimajor axis required to start mass transfer. They found that for higher eccentricity, the periastron separation must be smaller for mass transfer to commence. Lajoie & Sills (2011) presented results of SPH simulations of two main-sequence stars in eccentric orbits. They found episodes of accretion, with the rate peaking slightly after periastron passage. A small amount of mass (~5 per cent) is lost from the system in the process. CE simulations between giants and their companions tend to start with the companion already at the surface of the giant, thereby bypassing the entire pre-contact and Roche lobe contact phase (e.g. Passy et al. 2012; Ricker & Taam 2012).

In this paper, we carry out a limited set of hydrodynamic simulations of AGB stars with a companion in eccentric orbits and periods between ~10 and ~100 yr. We explore the effect of varying the periastron separation, initial eccentricity and companion mass. Since we consider the possibility that the A0V main-sequence companion was responsible for the interaction, we use a companion mass of $1.7\,M_\odot$ in most cases. However, we also consider the possibility of a higher and lower companion mass, in case the A0V star was not responsible for the interaction but instead a second companion interacted and merged with the AGB star to form the present day nebula. We concentrate on whether a disc is formed around the companion and whether this disc could drive the mass ejections deduced for the Rotten Egg Nebula. These simulations must be considered approximate because they neglect several potentially important effects. However, they include sufficient complexity to enable us to think

critically about these proposed models and suggest improvements and tests.

In particular, we will address the following questions. (i) How much mass is unbound from the system? (ii) What periastron separations will cause significant mass transfer on to the companion? (iii) If mass is transferred, will the interaction lead to an accretion disc around the companion that can launch a jet able to explain the lobes in the Rotten Egg Nebula? (iv) Will the interaction lead to a merger, and if not, can the interaction result in a wide orbit binary as is observed in the Rotten Egg Nebula?

In Section 2, we describe the method and initial setup for the simulations. Then in Section 3, we present the results: spinning up of the AGB star (Section 3.1), mass and longevity of the accretion disc (Section 3.2), the effect of a less and a more massive companion (Section 3.3), evolution of the orbital separation (Section 3.4), mass lost from the system (Section 3.5) and finally, numerical considerations (Section 3.6). In Section 4, we discuss the type of magnetic fields and jets that could arise from such discs. In Section 5, we discuss and conclude, while in Section 6, we summarize our results.

2 METHOD AND INITIAL SETUP

Using the one-dimensional stellar evolution code MESA (Modules for Experiments in Stellar Astrophysics; Paxton et al. 2011, 2013), we calculated the structure of an AGB star with a mass of $3.05\,M_\odot$ (zero-age main-sequence mass of $3.5\,M_\odot$, similar to that deduced for OH 231.8+4.2 by Jura & Morris 1985) and solar metallicity. This object has an age of ~3×10^8 yr, similar to the age of NGC 2437 which OH 231.8+4.2 belongs to (Mermilliod 1981). At this point in the stellar evolution, this AGB star has a radius $R_{\rm AGB} \sim$ 2.2 au. This star is then imported into a modified version of the three-dimensional hydrodynamics code ENZO (O'Shea et al. 2004; Passy et al. 2012; Bryan et al. 2014). This is a grid-based hydrodynamics code, using Cartesian coordinates. Using the Zeus module in ENZO, we evolve the hydrodynamics equations as in Passy et al. (2012). In particular, we evolve the internal energy rather than the total energy, and we calculate the gravitational potential using the Poisson equation.

We use a uniform grid with a resolution of 256^3 and a domain size of 4.4×10^{14} cm in all three directions in most cases. In one case, we use 512^3 cells (simulation no. 4hr in Table 1). In two cases, we simulate a larger volume of 5.3×10^{14} cm on a side and in order to keep the same grid-cell size we use a grid with 306^3 cells (simulations no. 2 and no. 8 in Table 1). The core of the AGB star is not resolved and is simulated as a point mass, as is the companion star (similarly to Passy et al. 2012). The AGB core point mass is $0.7\,M_\odot$, the same as the AGB star's carbon–oxygen core mass. In most of the simulations, the main-sequence companion has a mass of $1.7\,M_\odot$, consistent with the mass of an A0V main-sequence star. However, as it is possible that a third object was responsible for the interaction and merged with the AGB star, we have also run a simulation with a $0.6\,M_\odot$ companion and one with a $3\,M_\odot$ companion, both with eccentricities of 0.7, to investigate how the companion's mass affects the results.

While MESA has a very high resolution in one dimension and takes the microphysics into account, we use the three-dimensional ENZO code with a much coarser resolution, and with an ideal gas equation of state with $\gamma = 5/3$. As a consequence of the changed resolution, the use of a particle as the stellar core, and the different equation of state, a stable stellar model in MESA may not be stable in ENZO. After mapping the stellar model from MESA into ENZO, we fill the

Table 1. Overview of the initial setup and results for the simulations discussed in this paper. In all cases, the mass of the AGB star is $3.05\,M_\odot$, its radius is $R_{AGB} = 2.2\,au$. The simulation domain is a cube with sides 4.4×10^{14} cm long, except for simulations no. 2 and no. 8 (see the text), run at 256^3 resolution (except for simulations no. 2, no. 8 and no. 4hr). We refer to the labels given in this table when discussing the simulations in the text. The unbound material refers to the total unbound mass. The final separation and the accumulated unbound material are not available for simulations no. 3 and no. 6, since in these cases the orbit following the first periastron passage was sufficiently large that the companion left the grid. For these simulations, the period and eccentricity have been estimated based on the velocities after periastron passage.

Label no.	Comp. mass ($M_\odot$)	Initial separation (au)	Initial orbital period (yr)	Initial peri. sep. (R_{AGB})	Initial eccentricity	Smoothing length (cells)	Period after first peri. pass. (yr)	Eccentricity after peri. pass.	Disc mass after first peri. pass. ($M_\odot$)	Final sep. (Fig. 7) (au)	Unbound material[a] ($M_\odot$)	Unbound material[b] ($M_\odot$)
1	1.7	22	25.8	2.0	0.70	3.0	14	0.60	0.04	0.4	0.28	0.13
1ss[c]	1.7	22	25.8	2.0	0.70	1.5	12	0.62	0.02	0.4	0.31	0.14
2[d]	1.7	13.2	36.0	2.5	0.70	1.5	27	0.65	0.0004	0.6	0.35	0.12
							22	0.58	0.02[e]			
3	1.7	13.2	49.9	3.0	0.70	1.5	36	0.64	0.0	–	–	–
4	1.7	8.4	7.7	2.0	0.33	1.5	5	0.25	0.05	0.4	0.42	0.15
4hr[f]	1.7	8.4	7.7	2.0	0.33	3.0	6	0.29	0.03	0.2	0.16	0.12
5	1.7	12.1	12.0	2.0	0.50	1.5	9	0.40	0.02	0.4	0.42	0.16
6	1.7	13.2	134	2.0	0.90	1.5	55	0.80	0.002	–	–	–
7	0.6	13.2	19.2	1.5	0.7	3.0	12	0.48	0.001	0.3	0.14	0.08
8	3.0	22	32.0	2.5	0.7	1.5	16	0.65	0.06	1.0	0.22	0.12

Notes. [a] Including thermal energy in calculating the unbound mass.
[b] Not including thermal energy when calculating the unbound mass.
[c] 1.5 cells smoothing length.
[d] 306^3 resolution; bigger box, same cell size.
[e] After second periastron passage.
[f] 512^3 resolution.

surroundings with a low-density (four orders of magnitude less than the lowest density in the star) hot gas to match the stellar pressure at the surface. While damping the velocity field by a factor of 3 for each cycle, as done by Passy et al. (2012), the star is evolved without a companion for several dynamical time-scales so that a stable object is formed. Before inserting the companion, we evolve the star for several dynamical times without damping the velocities, to verify its stability. We also test the stability of the AGB structure in the ENZO domain by evolving the simulation with a single AGB star that is moving across the grid with a velocity typical of the orbital velocity of the primary in the binary system.

The MESA model outermost grid point is at the photosphere and has a density of $\sim 10^{-9}\,g\,cm^{-3}$. Hence, there is a sharp density jump from the photospheric density to the ambient background density four orders of magnitude lower. Over the stabilization time, despite the pressure support from the surrounding ambient medium, the stellar model diffuses out due to this sharp density jump (see Fig. 1). After stabilization, at a density of $10^{-10}\,g\,cm^{-3}$, the star is ~ 10 per cent larger than initially. Being at a larger radius, this material is less tightly bound and could more easily be dragged off during an interaction. Since very little mass resides in this puffed-up, low-density material, we do not, however, expect it to affect our simulations significantly. The low-density ambient medium causes a negligible drag on the companion as it moves through it.

The ambient medium has a high pressure, meant to equalize the outer part of the star initially. During the early part of the simulation, the ambient medium can therefore prevent low-pressure gas from expanding as much as it would naturally.

We insert the point mass companion into the computational domain and both stars (the giant with its core and the companion) are given velocities appropriate for the desired orbit. We do not stabilize the AGB star within the potential of the companion. This is only possible in the corotating frame, which is hard to implement for non-circular orbits. We determined that if the companion is initially
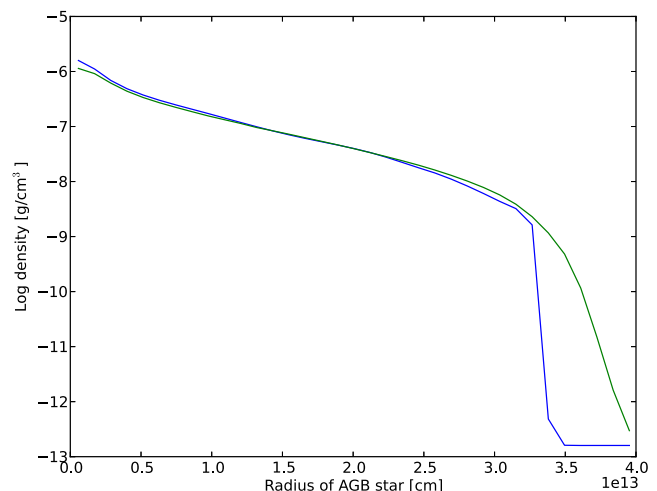

Figure 1. A comparison of the MESA AGB star density profile after mapping it into the ENZO computational domain (blue curve) and the same profile after 4 yr of relaxation when the structure stabilizes (green curve) for a simulation where the AGB star is single and moving across the grid, with a velocity similar to what it would have initially if there was a companion present.

placed at a separation $\gtrsim 6\,R_{AGB}$, it does not significantly affect the structure of the giant star. If the companion is inserted closer, the giant star is less distorted than if it had been allowed to adjust to the altered potential. As a consequence, the interaction during periastron passage in eccentric simulations like these will be weaker. This is primarily a problem in our less eccentric simulations (i.e. simulation no. 4, with an eccentricity of 0.33). This effect may influence the details of the simulations, but is unlikely to affect the main results, namely that the system soon enters a CE, and that little mass is unbound.

The gravitational potential created by a point mass is smoothed to prevent a singularity, as done by Sandquist et al. (1998):

$$\phi(r) = \frac{-GM}{\sqrt{r^2 + \epsilon^2\delta^2 \exp(-r^2/(\epsilon\delta)^2)}}; \qquad (1)$$

where G is the gravitational constant, M is the mass of the point particle, r is the distance from it, δ is the size of a cell and ϵ, the smoothing length, has a value of 1.5 or 3 (see Table 1). A smoothing length of 1.5 cells results in better resolution, but the potential gradients can be too steep for satisfactory energy conservation (discussed further in Section 3).

2.1 The Roche lobe radius

The aim of our simulation is to determine the type of interaction happening at or around the time of RLOF for an eccentric binary. Guided by the kinematic parameters of the Rotten Egg Nebula, which seems to have suffered an outburst ∼800 yr ago, we attempted to model a relatively long orbital period, but with a relatively short periastron distance. This can only be achieved with relatively high eccentricities. Nicholls & Wood (2012) found many high eccentricity, close binary stars with a giant primary, but not with an eccentricity value as high as we have selected for some of our simulations ($e \simeq 0.7$–0.9). We discuss the implications of our selections in Section 3.2.

Using the expression for the effective Roche lobe radius from Eggleton (1983):

$$r_L = \frac{0.49q^{2/3}}{0.6q^{2/3} + \ln[1 + q^{1/3}]}, \qquad (2)$$

with $q = M_d/M_a$ being the mass ratio of the two stars, we find that an $M_d = 3.05\,M_\odot$ donor star with an $M_a = 1.7\,M_\odot$ accreting companion ($q = 1.79$) has an effective Roche lobe radius of ≈0.43 times the separation of the two stars. Hence, for the $3.05\,M_\odot$ star to exactly fill its Roche lobe, the separation of the two stars must be 2.3 times the radius of the $3.05\,M_\odot$ star of 2.2 au. This expression, however, assumes that the stars are rotating synchronously and in circular orbits. In our case, the stars are not rotating initially, and are not in circular orbits. Sepinsky, Willems & Kalogera (2007) found that binary components rotating slower than the orbital velocity at periastron (as is likely to be our case at the first periastron passage) would have a Roche lobe radius up to 10 per cent larger than that given by the expression in equation (2). This can therefore reduce the mass transfer slightly. On the other hand, as we described above, the low-density outer layers of the star do diffuse out slightly (by about 10 per cent referring to a density contour of $10^{-10}\,\mathrm{g\,cm^{-3}}$; Fig. 1), making the star bigger and hence more likely to overflow its Roche lobe. These effects are opposite and may balance each other out to an extent.

3 RESULTS

We have carried out a number of simulations, whose initial configurations are summarized in Table 1. We choose simulation no. 1 (a $3.05\,M_\odot$ AGB star with a $1.7\,M_\odot$ companion, initial eccentricity of 0.7, a periastron separation of $2\,R_{AGB}$ and an orbital period of ∼26 yr) as an illustrative case and describe it below. In Sections 3.1–3.6, we give a quantitative account of the results and compare different simulations.

In Fig. 2, we present snapshots taken at different times showing density slices through the equatorial and perpendicular planes. During the first periastron passage, that takes place 8 yr after the start of the simulation, the AGB star overflows its Roche lobe and $0.04\,M_\odot$ is lost to a disc around the companion, while about $0.02\,M_\odot$ is lost from the simulation box (this mass is not necessarily unbound). In addition, a low-density stream of gas forms between the AGB star and the companion (see panel after $t = 18$ yr in Fig. 2). The stream and the plume of gas trailing the companion that can be seen in the figure after 18 yr are confined to the mid-plane of the simulation as they are in pressure equilibrium with the hot ambient medium. In a more realistic setup without the hot ambient medium, the plume would likely have been more puffed up. The companion's orbit is altered by the interaction and the companion with its disc return to periastron after only about 14 yr. The AGB star is at this point distorted (see Fig. 2), and its diameter, out to a density of $10^{-9}\,\mathrm{g\,cm^{-3}}$, is now between 10 and 30 per cent larger than it was initially, with much lower density material extending beyond that.

During the second periastron passage, more mass is dragged off the AGB star, some of which flows out of the simulation box (about $0.05\,M_\odot$ is lost from the simulation box during the next orbit as a consequence of this interaction), while $0.05\,M_\odot$ are captured by the companion, so that the disc mass grows to $0.09\,M_\odot$. The companion's orbit is altered further and the companion remains engulfed in the AGB star's envelope (see the panel at $t = 27$ yr in Fig. 2).

The CE proceeds in a manner qualitatively similar to previous simulations (Sandquist et al. 1998; Passy et al. 2012). We stop the simulation when the orbital in-spiral slows down, as described by Passy et al. (2012). We call mass that has a positive total energy unbound, and we calculate the total energy by both including or excluding the thermal energy i.e. gas is unbound if $E_k + E_{pot} + E_{th} > 0$ or $E_k + E_{pot} > 0$; note it has been argued that the enthalpy and not the thermal energy should be used (Ivanova & Chaichenets 2011), but this detail has no bearing on our conclusion. Including the thermal energy likely overestimates the amount of unbound mass. However, it is possible that part of the thermal energy will be converted into kinetic energy of the gas. Hence, ignoring the thermal energy in the computation of the unbound mass may underestimate the amount of unbound material. Therefore, we report the unbound mass calculated with both methods in Table 1. Finally, unbinding of mass generally occurs when gas interacts with the particles. As unbound gas travels outwards it may interact with bound material farther out, causing it to lose sufficient energy that it becomes bound, making it possible for the total amount of unbound gas on the grid to drop without mass being lost from the grid.

The high-resolution simulation (no. 4hr) ran over 8 d on 256 cores on the National Computational Infrastructure's Raijin[1] machine. Simulation no. 2 was the longest simulation of the lower resolution simulation set and took approximately one week on 128 cores. In addition, the stellar stabilization (Section 2) took approximately two days.

3.1 The AGB star's rotation

The interaction with the companion transfers orbital angular momentum to the AGB star. All CE interactions must take place between a companion and a spun-up star because a tidal interaction must have taken place on a shorter time-scale than the radial evolution of the binary, meaning that orbital angular momentum is transferred to the primary by tidal dissipation as the companion is

---

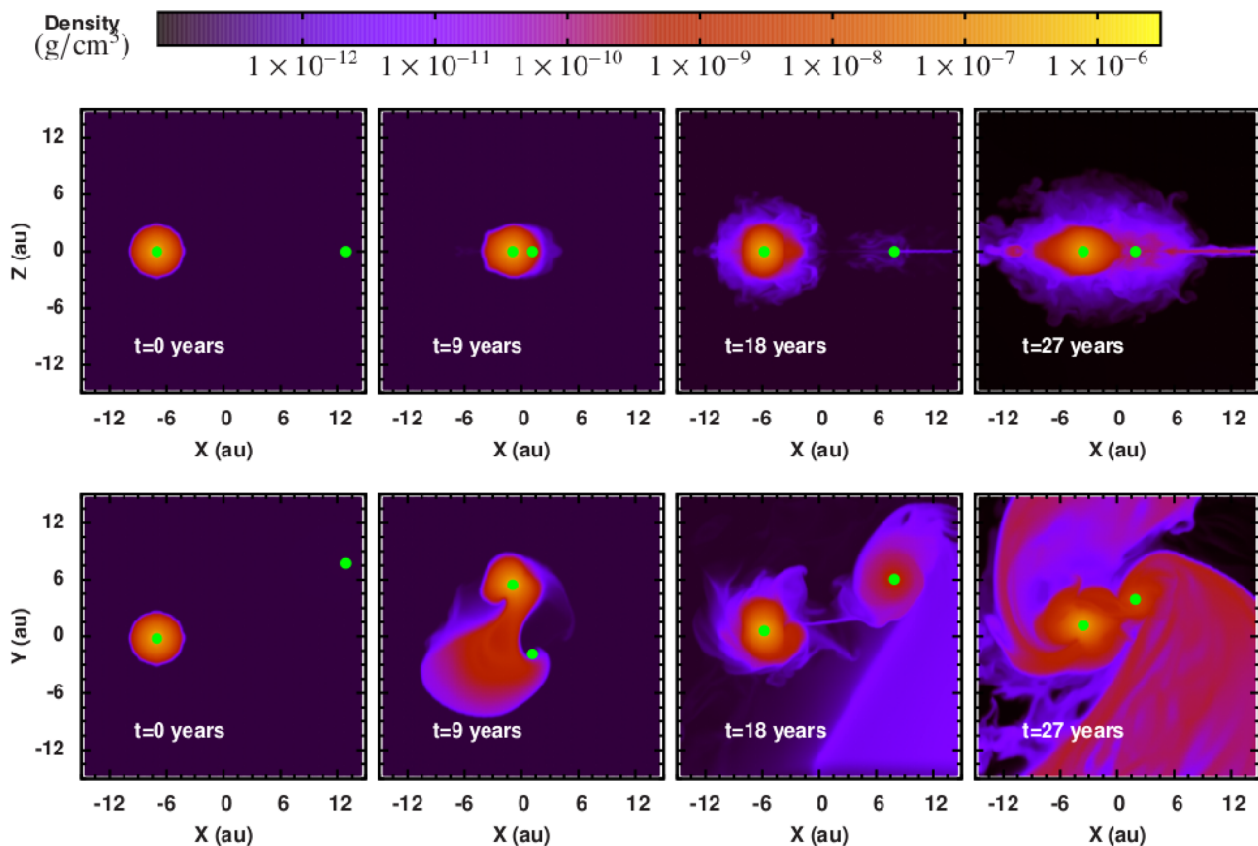[1] nci.org.au/nci-systems/national-facility/peak-system/raijin/

Figure 2. Snapshots showing density slices perpendicular to the equatorial plane (top panel) and along the equatorial plane, (bottom panels) at four different times in simulation no. 1 (Table 1). The green dots are the particles positions projected on to the plane.

brought into contact. However, it is non-trivial to simulate an interaction with a rotating giant because setting up a stable, rotating star in the 3D computational domain requires, once again, the corotating frame. In the corotating frame, there are no orbital velocities. Any velocity can therefore be dampened as they arise from instabilities. In a rotating giant the velocity contrast between the companion and the envelope gas is smaller, which will result in a lower gravitational drag force experienced by the companion. This will likely change the nature of the interaction. Sandquist et al. (1998) reported that setting their $3 M_\odot$ AGB primary in synchronous rotation with the $0.4 M_\odot$ companion at a distance of 2×10^{13} cm (equivalent to $1.44 R_{star}$) did not alter the outcome of the CE interaction compared to a situation with no rotation.

We investigate the velocity field of the AGB star, in the stellar core's frame of reference, after 20 yr of simulation time, 12 yr after the first periastron passage, corresponding to 6.5 AGB stars dynamical times. In order to quantify the rotational velocity, we find the velocity at different constant radii and constant densities in the equatorial plane in the envelope. The results are given in Table 2. The highest velocities are found at low densities and large radii, as expected since those layers suffered the strongest interaction. How the velocity profile will redistribute depends greatly on the stellar structure as well as its magnetic fields (Cantiello et al. 2014) and we cannot hope to reproduce it here. However, the amount of angular momentum received by the star from the spin-orbit interaction is likely reasonably accurate at the angular momentum conservation level observed.

Shown in Fig. 3 are filled contour plots of the logarithm of the density and of the magnitude of the velocity field, overplotted with

Table 2. The velocity modulus in the equatorial plane of the AGB star's envelope, in the frame of reference of the core of the AGB star, after 20 yr in simulation no. 1, at different radii.

Radius (au)	Density (10^{-10} g cm^{-3})	Velocity (km s^{-1})	Mean velocity (km s^{-1})
0.9–1.1	500–10 000	0.4 – –3	2
1.7–2.0	80–100	2–8	5
2.1–2.3	2–80	5–15	8
2.6–3.0	8–10	5–20	12

the velocity vectors. In both cases, the pink curve indicates densities between 8×10^{-9} g cm^{-3} and 10^{-8} g cm^{-3}, a level at which we found a velocity 2–8 km s^{-1} (see Table 2). In Fig. 4, we show the specific angular momentum as a function of the logarithm of the density. The highest specific angular momenta ($>10^{20}$ cm^2 s^{-1}) are found at densities below $\sim 10^{-9}$ g cm^{-3}. This lower density material is farther from the centre of the star, where the highest velocities are found. At densities of $\sim 10^{-8}$ g cm^{-3} there are also some regions with negative specific angular momentum. This is caused by an apparent rotation in the star's envelope at those densities. This is vaguely apparent by looking at the velocity vectors in Fig. 3 to the lower left of the centre of the star. In conclusion, the star is spun up by the first interaction such that the velocity contrast between the companion and the gas at the next periastron passage will be smaller and the strength of the interaction at the start of the CE could be reduced.
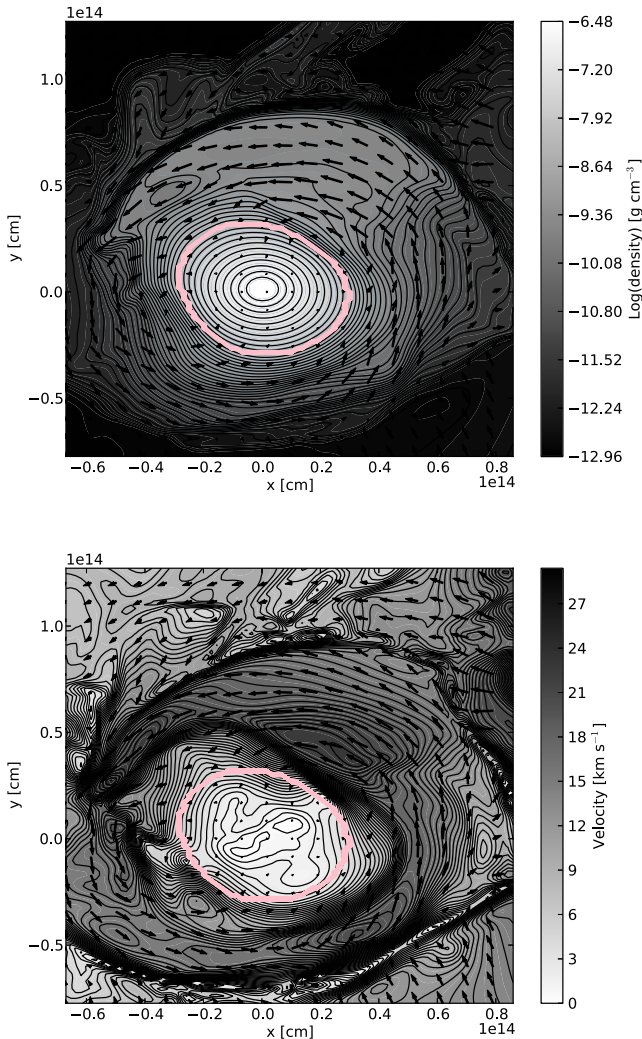
Figure 3. The logarithm of density (top), and the absolute value of the velocity vector field in the frame of reference of the AGB star's core (bottom), in the orbital plane, 20 yr into the simulation (about 12 yr after the first periastron passage), overplotted with the velocity vectors on that plane, drawn every five zones in the grid. The pink curve indicates densities between $8 \times 10^{-9}\,\mathrm{g\,cm^{-3}}$ and $10^{-8}\,\mathrm{g\,cm^{-3}}$. The core of the AGB star is at (0,0) in the figure.

3.2 The accretion disc

The jets that formed the Rotten Egg Nebula must have been massive and fast. Our aim is to determine whether the conditions necessary for launching such jets can arise during the modelled interaction.

Here we discuss the formation of accretion discs at the time of RLOF, but acknowledge that once formed, the disc dynamics will be dictated by cooling and magnetic fields, neither of which is included in our simulation. We therefore use primarily the mass of the disc after RLOF to anchor our discussion, leaving all other conclusions to an analytical study in Section 4. There is an uncertainty in the disc mass since some mass is lost from the grid following the first periastron passage. However, the lost mass is substantially less than the mass of the disc ($0.04\,\mathrm{M_\odot}$) in simulation no. 1, and most of it is kinematically unlikely to make it into the disc before the next periastron passage (see Fig. 5). Hence, the uncertainty in the disc
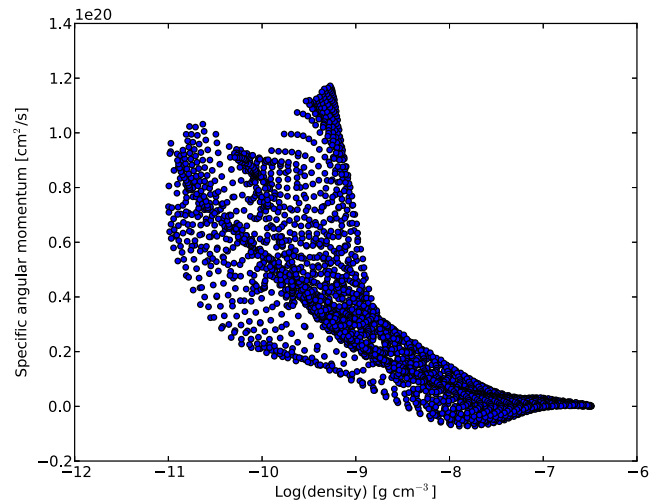

Figure 4. The specific angular momentum of the AGB star in the orbital plane as a function of the logarithm of the gas density, for simulation no. 1 after 20 yr. The slightly negative specific angular momenta found around $10^{-8}\,\mathrm{g\,cm^{-3}}$ show counter rotation in the star at those densities. We only plot the angular momentum at densities larger than $10^{-11}\,\mathrm{g\,cm^{-3}}$.

mass following the first periastron passage in simulation no. 1 is small.

As we have discussed in Section 2.1 we have adopted a high value of the eccentricity to maximize the orbital period, while maintaining a periastron distance that would allow mass transfer. Hence the longest our discs have to launch a jet after they form is 55 yr (simulation no. 6) or 27 yr for a simulation with a more realistic initial eccentricity (simulation no. 2), although those discs contained very little mass. The longest time for a disc containing a reasonable amount of mass ($\gtrsim 0.01\,\mathrm{M_\odot}$) to launch jets is 22 yr (simulation no. 2 after the second periastron passage). All these times should be regarded as upper limits since for lower, more reasonable values of the eccentricity, these times would be shorter.

The masses of the discs formed in our simulations are $<0.06\,\mathrm{M_\odot}$. The disc density structure is shown in Fig. 6 for simulation no. 1. The orbital period within that disc is 0.5 yr at a radius of 5×10^{12} cm or 0.33 au, or 3 cells from the companion particle. Therefore in the $\sim$10 yr available to form a jet, the disc at that radius completes 20 revolutions, and many more at the smaller radii close to the stellar surface from which a fast jet will be driven (e.g. Zanni & Ferreira 2013; Staff et al. 2015).

We can gauge the mass accretion rate on to the disc from the following argument. When the companion approaches the first periastron passage, the AGB star gets severely distorted and mass transfers to the companion. However, it is only some 2 yr later that this mass begins to engulf the companion, which has now passed periastron (see Fig. 5). 4–5 yr past first periastron passage, one can start recognizing a disc around the companion, which is linked to the AGB star through a stream of gas. As the companion moves away from the AGB star, the disc becomes more prominent while the stream weakens. Most of the $0.04\,\mathrm{M_\odot}$ transferred to the disc arrives shortly after periastron passage. The mass transfer to the disc varies with a maximum value of $\sim 0.01\,\mathrm{M_\odot\,yr^{-1}}$ during this time.

The simulation with $2\,\mathrm{R_{AGB}}$ periastron separation was also run with eccentricities of 0.33, 0.5, and 0.9 (simulations no. 4, no. 5, and no. 6 in Table 1). A lower eccentricity results in a higher disc mass after the first periastron passage. This is relatively easy to
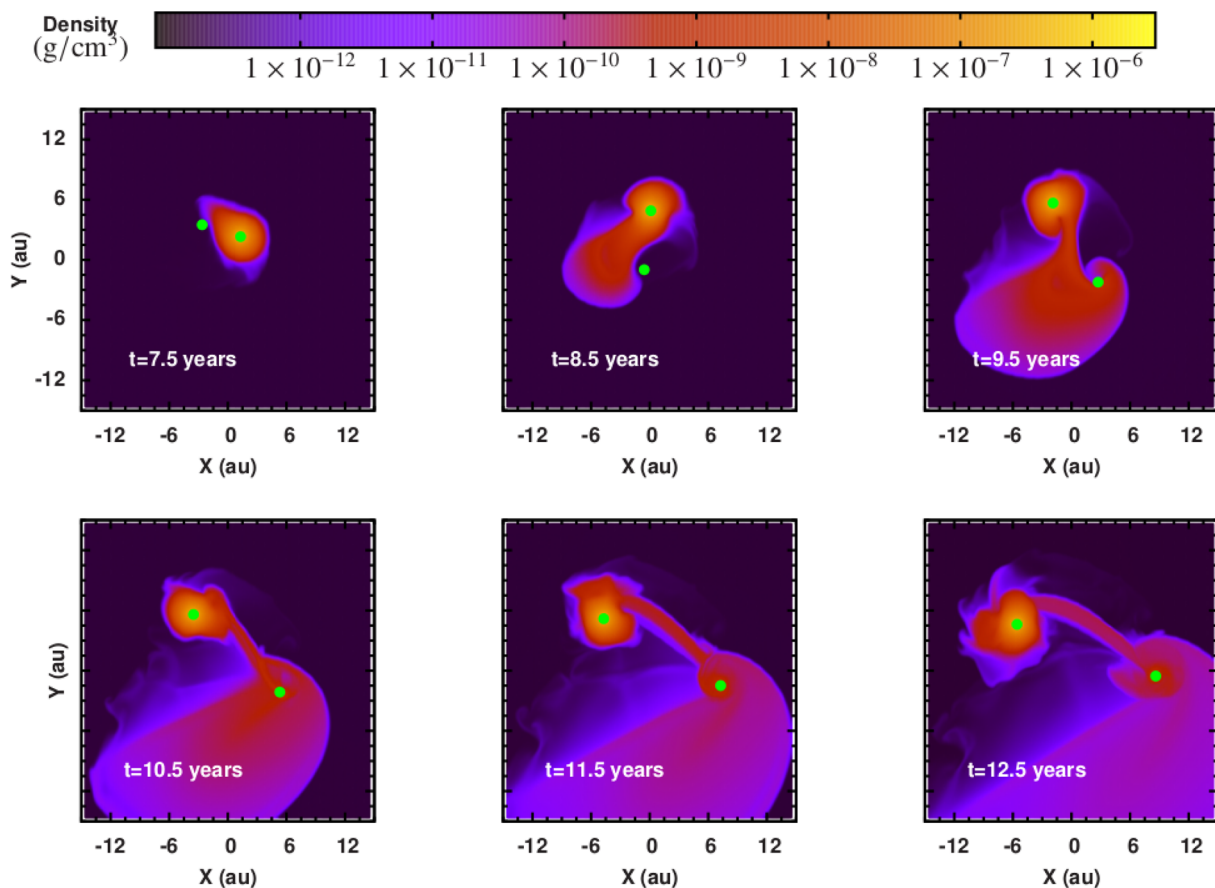
Figure 5. Snapshots showing density slices in the equatorial plane around the time of the first periastron passage for simulation no. 1. The green dots are the positions of the particles.

understand: a lower eccentricity for a given periastron separation means a shorter period. Relatively more time is spent at close proximity for the more circular orbit. In simulation no. 4, the lowest eccentricity simulated, the system almost forms a CE after the first periastron passage.

3.3 The effect of varying the companion mass

In most of our simulations, the companion mass was $1.7 \, M_\odot$, because the companion in the Rotten Egg Nebula is an A0V star. However, since we find that upon mass transfer, a CE interaction always follows within a few additional orbits, it is difficult to explain how the companion can now be at a separation >10 au. Other companion masses are therefore possible, since the A0V companion may not have been responsible for the interaction, but instead a third object may have interacted with the AGB star and merged. This third companion must have been less massive than the AGB star's initial mass of $3.5 \, M_\odot$, or otherwise it would have evolved sooner than the AGB star. We therefore ran one simulation with a companion mass of $0.6 \, M_\odot$ (simulation no. 7), and another with a companion mass of $3 \, M_\odot$ (simulation no. 8), both with an eccentricity of 0.7.

A lower companion mass means that the periastron separation must be smaller in order for any significant mass transfer to occur. For equal eccentricity, the orbital period will be shorter and the system enters a CE phase sooner (when compared to simulation no. 1). For a larger companion mass, a larger initial periastron separation leads to a similar mass transfer, but with a longer period following the first periastron passage. Interestingly, both a smaller and a larger companion mass than $1.7 \, M_\odot$ lead to less mass being unbound from the system (see Table 1). The larger final separation in simulation no. 8 (see below) may explain why less mass was unbound in the simulation with the more massive companion.

3.4 Orbital stability and the evolution of the orbital separation

3.4.1 Early evolution

Simulations were also run with different periastron separations of $2.5 \, R_{AGB}$ and $3 \, R_{AGB}$ (simulations no. 2 and no. 3 in Table 1). In simulation no. 3, the AGB star only receives a small perturbation during periastron passage, but no mass is transferred. The simulation box is too small to capture the whole orbit, but we could estimate the orbit based on the velocity vector before the companion leaves the box after the periastron passage. As it turns out, the orbit is barely altered by the first periastron passage. For simulation no. 2, there was a small amount of mass transfer during the first periastron passage, which resulted in a $4 \times 10^{-4} \, M_\odot$ disc surrounding the companion. The orbit was altered and the orbital period and eccentricity changed from 36 to 27 yr and from 0.7 to 0.65, respectively. During the second periastron passage, $0.02 \, M_\odot$ were transferred to the disc and the orbit was altered further (period and eccentricity changed to 22 yr and 0.58, respectively), eventually leading to a CE after four periastron passages.

Based on these simulations, we conclude that a periastron separation of roughly $2.5 \, R_{AGB}$ is a critical separation for a companion mass of $1.7 \, M_\odot$. For periastron separations larger than this value
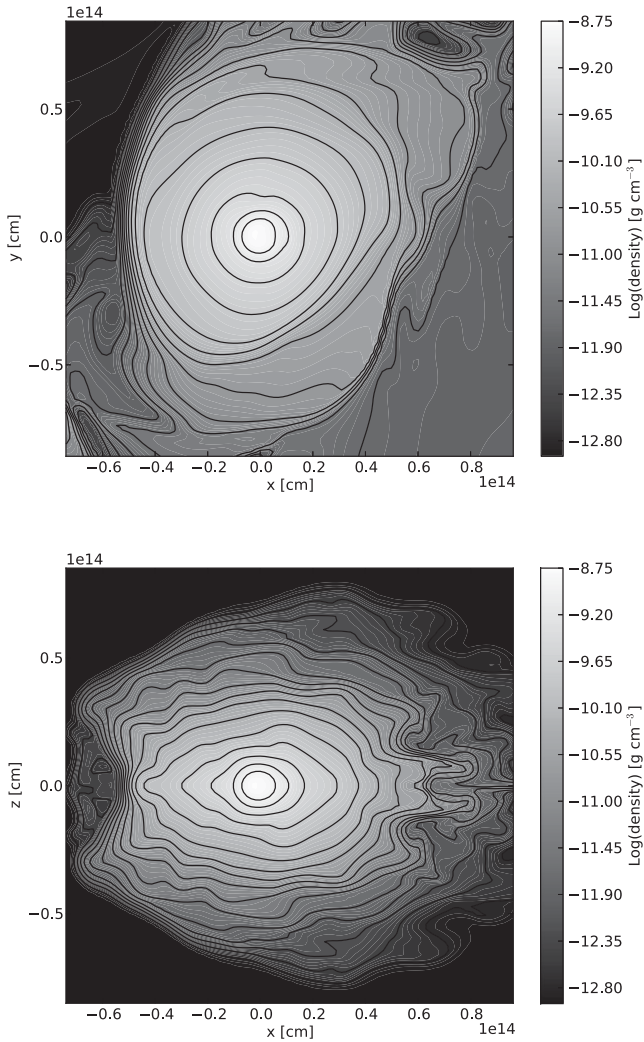
Figure 6. A density slice in the disc's mid-plane (upper panel), and in the perpendicular plane (lower panel) 12 yr after the first periastron passage.

the orbit is stable over longer, tidal time-scales. For smaller separations, we observe instead a stronger interaction that likely results in outburst type variability and leads to a CE after one or two progressively smaller orbits. In some sense, increasing the periastron separation while maintaining the eccentricity unchanged has a similar effect to increasing the eccentricity while maintaining the initial periastron separation unchanged. Less mass is transferred during the periastron passage, and the system takes longer to evolve into a CE.

For the simulations with more than one periastron passage, we find that the eccentricity decreases for each passage (most noticeable for simulation no. 2 in Fig. 7), as expected (Passy et al. 2012).

3.4.2 Final separation

In Fig. 7, we plot the separation between the core of the AGB star and the companion as a function of time for all simulations that enter a CE. Initially, the separation is reduced, as the objects approach periastron. The final separations are about 0.4 au for all of simulations, except simulation no. 2, which has a larger final separation of ~0.6 au, the higher resolution simulation no. 4hr with a final separation of ~0.2 au, and simulation no. 8 with a final separation
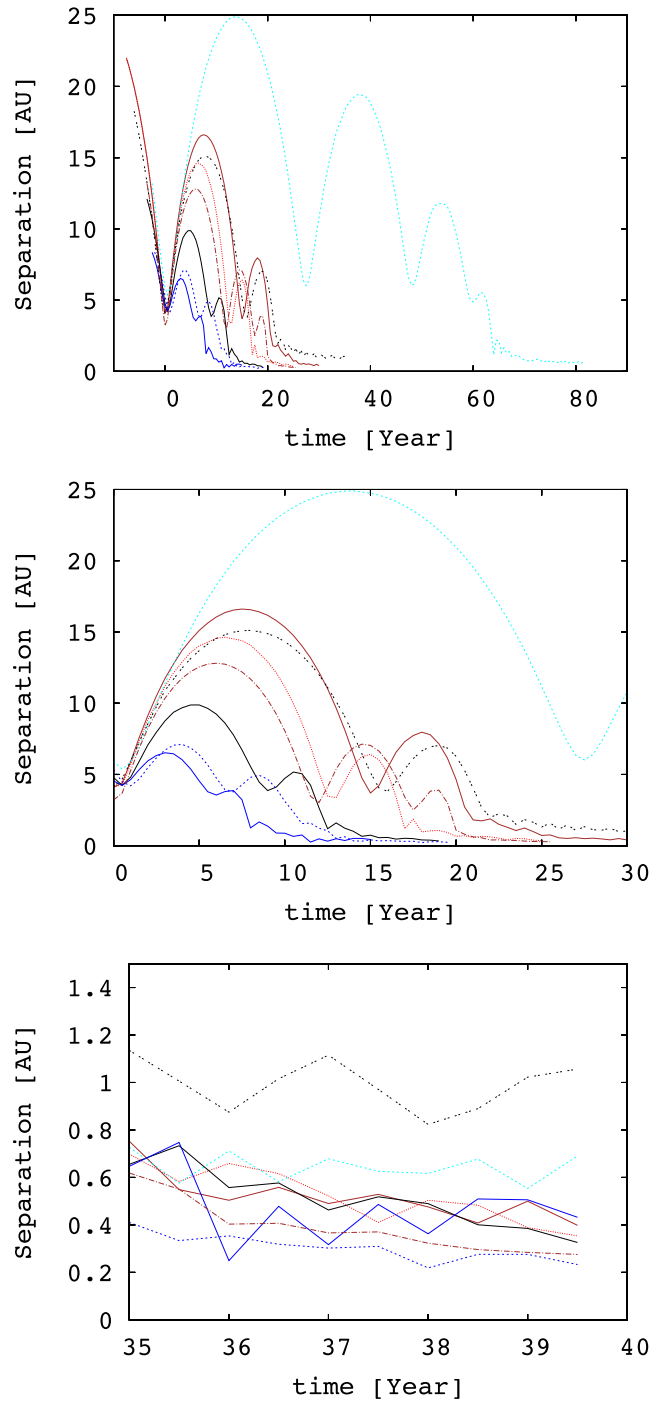
Figure 7. Upper panel: the separation between the core of the AGB star and the companion as a function of time. Each curve has been shifted so that the zero-time point coincides with the first periastron passage. Middle panel: zoom-in on the top panel between 0 and 30 yr, to better show the details of that part of the figure. Lower panel: zoom-in on the final separation between the core of the AGB star and the companion. In this plot, the curves have been shifted left or right so as to end at the same time. Dotted red line: simulation no. 1ss (with 1.5 cells smoothing length); brown solid line: simulation no. 1 (with 3 cells smoothing length); blue solid line: simulation no. 4' blue dashed line: simulation no. 4hr; black line: simulation no. 5; short-dashed cyan line: simulation no. 2; brown dash–dotted line: simulation no. 7; black dash–dashed line: simulation no. 8 (see Table 1).
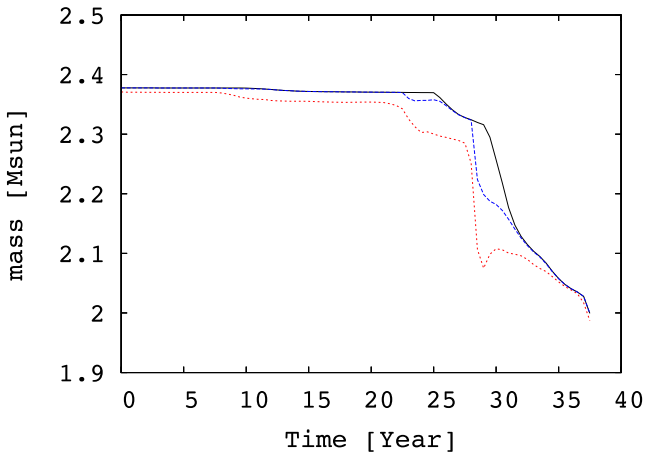
Figure 8. Solid black curve: the total gas mass on the grid (i.e. excluding the mass of the particles) for simulation no. 1. Dotted red curve: the total bound gas mass on the grid, including the thermal energy in the calculation of unbound mass. Dashed blue curve: the total bound gas mass on the grid, excluding the thermal energy calculating the unbound mass.

of ∼1 au. These separations are only upper limits, however, because the gravitational smoothing length of 3 cells corresponds to 0.34 au for the 256^3 resolution (simulation no. 1 and no. 7) and 0.17 au for the other 256^3 simulations with 1.5 cells smoothing length, as well as the 512^3 simulation with 3 cells smoothing length (simulation no. 4hr). Comparing simulation no. 1 to simulation no. 1ss shows that a factor of 2 decrease in smoothing length also does not change the result, although both values are within a factor of two of the final orbital radius. However, the comparison of simulation no. 4 to simulation no. 4hr shows that increasing the numerical resolution by a factor of 2, even with constant smoothing length, causes a factor of 2 decrease in the final orbital radius. This suggests that resolution of the orbit rather than smoothing length is the dominant factor determining final radius (also see Passy et al. 2012). The final radius reached with these physical assumptions will ultimately need to be determined by adaptive mesh simulations.

We do note that the stabilization separation is larger (0.6 au) for the simulation that starts with more angular momentum (simulation no. 2). We attribute this trend to the fact that more angular momentum is transferred to the primary, which is spun up as a result. This has the effect of lessening the strength of the interaction with the companion, although this is still a poorly resolved result.

3.5 Mass-loss

An outstanding question in all binary interactions, including mergers, is how much mass is lost from the system. In CE interactions resulting in close binaries we know that the entire envelope of the giant star must be ejected. However, simulations (Rasio & Livio 1996; Sandquist et al. 1998; Ricker & Taam 2012; Passy et al. 2012) have typically found that most envelope mass is still bound to the system by the time the orbital in-fall stabilizes, opening the possibility that either gas falls back rekindling the interaction, or pointing to the fact that an additional energy source must be available (Ivanova, Justham & Podsiadlowski 2015; Nandez, Ivanova & Lombardi 2015).

Because of the limited size of the grid, mass flows out of the computational domain, especially towards the end of the simulations. Fig. 8 shows the total gas mass on the grid (i.e. excluding the mass of the particles) and the bound gas mass on the grid for simulation
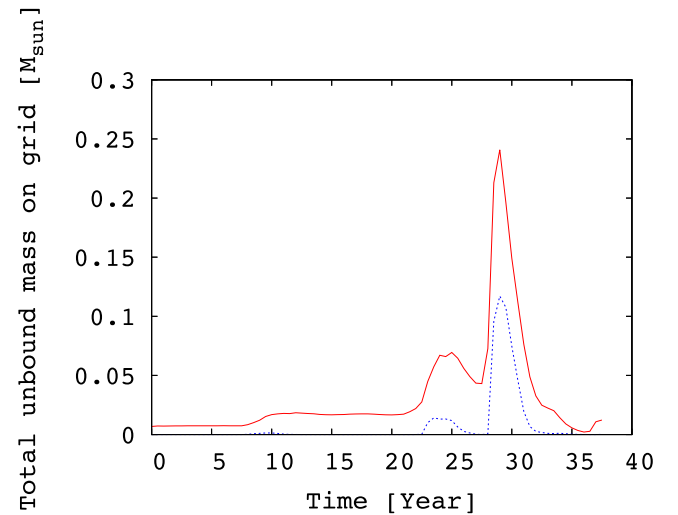

Figure 9. The total unbound mass on the grid as a function of time for simulation no. 1, including the thermal energy term when calculating the unbound mass (solid red curve) or excluding it (dashed blue curve). Rises in the curves correspond to unbinding events, while drops occur when unbound mass flows off the grid (cf. Fig. 8).

no. 1. As can be seen, most of the mass remains bound. In Fig. 9 we show the total unbound gas mass on the grid as a function of time for simulation no. 1.

Both the bound and the unbound mass shown in Figs 8 and 9 have been calculated both including and excluding the thermal energy term. After the first periastron passage (∼8 yr), we find that about $0.02\,M_\odot$ is unbound when including the thermal energy, and only a negligible amount when excluding it. After the second periastron passage, the unbound mass reaches about $0.07\,M_\odot$ ($0.01\,M_\odot$, excluding the thermal energy) before dropping by about $0.03\,M_\odot$ ($0.01\,M_\odot$), as some unbound mass leaves the computational domain. Then the unbound mass grows by about $0.21\,M_\odot$ ($0.10\,M_\odot$) to reach a peak of about $0.25\,M_\odot$ ($0.12\,M_\odot$). Summing up, $0.28\,M_\odot$ ($0.13\,M_\odot$) of gas in total was unbound, or just above 10 per cent (5 per cent) of the AGB star's envelope. In Fig. 9 a decreasing unbound mass is caused by unbound mass leaving the grid or by unbound mass losing energy and becoming bound, for instance by colliding with bound of gas. Following the final periastron passage, much mass, both bound and unbound, flows off the grid. Eventually the unbound mass drops to zero, indicating that no more mass is being unbound as the separation stabilizes. Since the final separation is an upper limit, we must conclude that the unbound mass in our simulations is a lower limit.

3.6 Numerical considerations

3.6.1 Energy conservation

No grid simulation of this kind conserves energy perfectly (see e.g., Sandquist et al. 1998; Passy et al. 2012). This is in part due to the contribution from self-gravity being added as a source term in the momentum and the energy equations (equations 2 and 3 in Bryan et al. 2014). In other words, these equations are written and solved in non-conservative form. Therefore, momentum and energy are not conserved to roundoff error and the level of non-conservation can vary depending on how dominant self-gravity is for the evolution of the system. For more details, see Jiang et al. (2013). The steeper the potential gradient, the worse the conservation.

Checking for energy conservation is notoriously difficult in grid simulations with outflowing boundary conditions because mass and energy are lost from the computational domain. This situation is particularly difficult to handle in our case. Our low-density, high-temperature 'vacuum' (see Section 2) has a substantial amount of thermal energy, which leaves the grid even before substantial mass starts to flow out. Passy et al. (2012) used their SPH calculation to determine that energy and angular momentum were reasonably conserved. They did not check their grid simulations for energy conservation because the results of grid and SPH simulations, for the same input parameters, were comparable.

In Fig. 10 we show the energy components of simulation no. 1 compared to no. 1ss (which has a smaller smoothing length of 1.5 cells, for which energy conservation tends to be worse). The thermal energy (cyan curve) is dominated to large extent by the hot, low-density gas initially permeating the computational domain (which we call vacuum; Passy et al. 2012). This low-density medium contains substantial thermal energy despite its low total mass. In addition, some of the AGB star's thermal energy is converted into potential energy as the star expands, adding to the decline in the thermal energy. By the time of the first periastron passage at $t \approx$ 8 yr, when substantial mass starts flowing out of the computational domain, making it difficult to track energy conservation, the simulation box has lost 2×10^{-4} M$_\odot$ of this hot, low-density ambient gas. The thermal energy of this lost gas is about 10^{45} erg for both simulations, explaining the initial drop in the thermal energy.

Despite the drop in thermal energy, the total energy in simulation no. 1 shows a slight increase over a four year period around the first periastron passage. This increase is about 5×10^{44} erg over these four years, and because it is small compared to the scale of the plot in Fig. 10 it is not apparent in the figure. During this time, the total energy should in fact have decreased by about 5×10^{44} erg because of the hot, low-density ambient gas left the grid. The error over this 4-yr period is therefore $\sim 1 \times 10^{45}$ erg, which we can compare to the total initial potential energy[2] of $\sim 8 \times 10^{46}$ erg. The relative error in the total energy over this 4-yr period is therefore ~ 1 per cent. In simulation no. 1ss, with a smaller smoothing length of 1.5 cells, we find a larger error in the energy conservation of 4 per cent over the same period. We note however that energy non-conservation in simulation no. 1 is only apparent during the 4 yr around the first periastron passage, when the interaction is strongest. We therefore do not expect this non-conservation to grow linearly with time, at least not for the period of time between 10 and 20 years, when the primary core and companion are not interacting strongly. Indeed, for the first 9 yr of simulation no. 1, we find that the error in the energy conservation is also ~ 1 per cent, while in simulation no. 1ss it is ~ 8 per cent over the first ten years.

From approximately 10 yr after the start of the simulations, sufficient mass leaves the grid that energy conservation cannot be tracked any longer. We note that in simulation no. 1ss, with the shorter smoothing length, the evolution proceeds faster as expected from the fact that the gravitational interaction between particles and gas is stronger. Although the energy conservation is worse, the strength of the interaction is more realistic. Overall, however, the outcome of the simulations are very similar, when considering our

[2] We compare the change in total energy to the initial stellar potential energy rather than the initial total energy in the computational domain. The stellar potential energy can be considered representative of the stellar energy because the kinetic and internal contributions are small (the thermal energy in the computational domain is dominated by the energy of the hot vacuum).
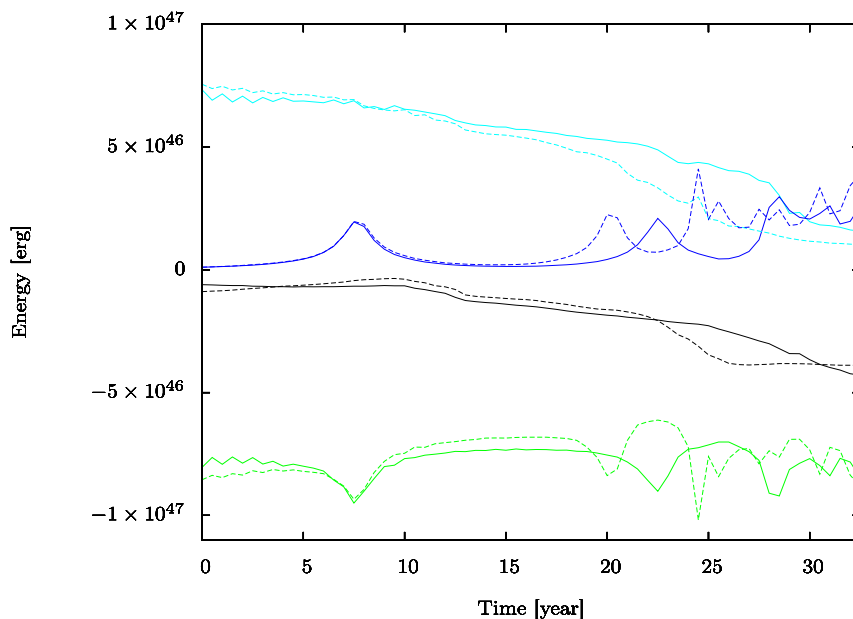
tolerance. In simulation no. 1ss the second periastron passage takes place ~ 2 yr earlier and the disc mass is half that of simulation no. 1. The amount of unbound gas and the post-CE separations are very similar.

3.6.2 Numerical resolution

We carried out a simulation (no. 4hr) equivalent to simulation no. 4, but with a resolution of 512^3 instead of 256^3. The smoothing length of simulation no. 4hr was 3 cells, compared to the 1.5 cells of simulation no. 4. In this way, the strength of the interaction between particles and gas is preserved.

The higher resolution simulation no. 4hr has a slightly weaker interaction at periastron, causing slightly less mass to be transferred during the first periastron passage and therefore a slightly longer orbital period following that (see Table 1). Simulation no. 4hr unbinds much less mass than simulation no. 4 (0.16 versus 0.42 M$_\odot$) if considering the thermal energy in deciding what mass is unbound, however, if only considering whether gas has reached the escape velocity when determining if mass is unbound, the difference is found to be less (0.12 versus 0.15 M$_\odot$). The lower final separation in simulation no. 4hr (0.2 versus 0.4 au) indicates that the resolution affects the final separation, as expected (Passy et al. 2012) and discussed above.

However, the exact role played by the combination of resolution and smoothing length in slowing down the in-spiral is not simple. Within a particle's smoothing length, the gradient of the gravitational potential is zero. This therefore affects how close the particles can reliably be simulated. For both simulations no. 4 and no. 4hr, the respective smoothing lengths are equivalent to 2.6×10^{12} cm $= 0.17$ au, only slightly smaller than the 0.2 au separation reached by simulation no. 4hr. We also know from comparing simulations no. 1 and no. 1ss that the smoothing length per se did not affect the final separation. It may be that the larger growth in potential energy in simulation no. 1ss than in simulation no. 1 due to energy non-conservation leaves the companion at a larger separation than what would have resulted had the energy been perfectly conserved.

Pending additional tests of how the gravitational friction that dictates the extent of the inspiral depends on different numerical aspects, we can only say that the simulation is not formally converged. This said, and in light of the other tests we have carried out and of the fact that we are, at this time, interested primarily in an order of magnitude answer, we did not carry out additional convergence testing.

3.6.3 The adiabatic assumption

Our simulation is carried out assuming an adiabatic gas. This is appropriate when simulating the fast, dynamical inspiral phase of a CE interaction, but less so for the current simulations that take place over 20–30 yr, which is 6–10 AGB star dynamical times and comparable to the ~ 45 year AGB star thermal time-scale. We here make a rough estimate of the energy that would be lost due to radiation, to estimate how appropriate the adiabatic assumption is in our case.

Following the first periastron passage in simulation no. 1, the AGB star approximately doubles its radius. If we assume that it retains the same surface temperature, then we find that during the 14 yr between the first and the second periastron passages the star would radiate 10^{47} ergs. This is a factor 4 larger than the energy radiated by the unperturbed star over this 14-yr time period

Figure 10. Energy components for simulation no. 1 (solid curves) and simulation no. 1ss (dashed curves) (3 cells and 1.5 cells smoothing length, respectively). The blue curve is the kinetic energy of the gas in the AGB star's envelope and of the particles, the cyan curve is the thermal energy in the box, the green curve is the total potential energy of the gas–gas, gas–particles and particle-particle, and the black curve is the total energy (kinetic+potential+thermal) of the whole system in the computational domain.

$(2.5 \times 10^{46}$ ergs). The thermal energy of the unperturbed star initially is 4×10^{46} ergs. Hence, the star does not have sufficient energy to maintain this luminosity for the whole period between the two first periastron passages. In reality, the photospheric temperature of the expanded AGB star may be lower than its initial effective temperature. Considering as a lower limit that the luminosity of the expanding AGB star remains the same, its photospheric temperature must decrease to ~2060 K (from the initial temperature of 2920 K). Mira stars have a pulsation cycle of approximately a year with a radius excursion of a factor of ~2, during which time the photospheric temperature decreases by approximately the same factor (Ireland, Scholz & Wood 2011). If this were the case in our situation the luminosity of the expanded AGB star would be approximately one-tenth that of the original star. We conclude that the adiabatic assumption is likely a borderline assumption in this case and may, during the second periastron passage, have contributed somewhat to a larger AGB star than would result if energy losses were included.

The disc forming around the companion after the first periastron passage in simulation no. 1 has a mass of $0.04\,\mathrm{M_\odot}$, but it has a radius of several au. However, with such low mass, the disc possesses little thermal energy compared to the star, and it is therefore likely that its photosphere would cool quickly. Hence, once again we may be overestimating the interaction during the second periastron passage since both the AGB star and the disc may be thinner than we simulated. However, since the periastron separation decreases between the first two passages (see Fig. 7), we conclude that although the simulated interaction at the second passage might be stronger than in nature, so the number of orbital periods before the CE phase may be lower, it is unlikely to be lengthened substantially.

4 POSSIBLE JET PARAMETERS

The outflows in the Rotten Egg Nebula have velocities of 200–400 km s^{-1} (Desmurs 2012). Sánchez Contreras et al. (2004) sug-

gested that these lobes had been inflated by jets with velocities of the order 500–1000 km s^{-1}. Soker & Kashi (2012) found that, to be consistent with the energy and momentum measurements of Alcolea et al. (2001), the jets must have had a mass of 0.01–$0.02\,\mathrm{M_\odot}$. The jets then interacted with the circumbinary gas to create the present-day lobes with their slower velocities.

If we assume that the jets originate in a disc around the companion, and that the outflow velocity equals the escape velocity ($v_{\mathrm{esc}} = \sqrt{2GM/r}$, with $M = 1.7\,\mathrm{M_\odot}$ being the mass of the companion and r being the distance from it) at the launch radius, then we find that the jet launching radius must be $2.6\,\mathrm{R_\odot}$ to reach a velocity of 500 km s^{-1}. The lower limit for the disc launch radius is the stellar radius, $\sim1.5\,\mathrm{R_\odot}$ for a $1.7\,\mathrm{M_\odot}$ main-sequence star, and the maximum jet speed achievable is ~655 km s^{-1}.

The maximum accretion rate into the disc at the time of RLOF in our simulations is $0.01\,\mathrm{M_\odot}$ yr^{-1} (Section 3.2). If this were the accretion rate on to the companion it would be entirely plausible for a jet of $0.02\,\mathrm{M_\odot}$ to be launched over a decade, assuming that 10–40 per cent of the accreted mass is launched into a jet (such ratios are typical for protostellar jets, see for instance Pudritz, Hardcastle & Gabuzda 2012; Federrath et al. 2014). However, such an accretion rate on to the secondary would generate a luminosity above the Eddington limit. The Eddington luminosity

$$L_{\mathrm{Edd}} = \frac{4\pi GMm_{\mathrm{p}}c}{\sigma_{\mathrm{T}}} = 5.4 \times 10^4 \,\mathrm{L_\odot} \times \left(\frac{M}{1.7\,\mathrm{M_\odot}}\right), \tag{3}$$

where m_{p} is the proton mass and σ_{T} is the Thomson scattering cross-section. This translates into an upper limit for the accretion rate of

$$\dot{M} = (0.002 - 0.003\,\mathrm{M_\odot}\,\mathrm{yr}^{-1})\left(\frac{L}{54\,000\,\mathrm{L_\odot}}\right)$$

$$\times \left(\frac{r}{2.6 - 1.5\,\mathrm{R_\odot}}\right)\left(\frac{1.7\,\mathrm{M_\odot}}{M}\right), \tag{4}$$
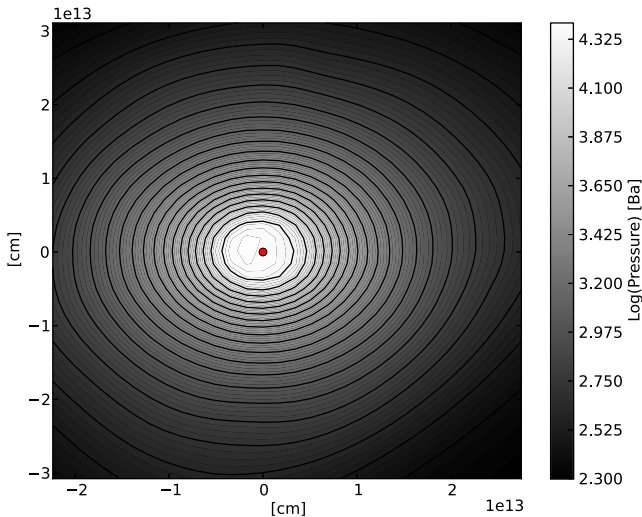
Figure 11. Contour plot showing the logarithm of the pressure in the disc mid-plane around the companion, 20 yr into simulation no. 1. The position of the companion is indicated by a red circle.

Assuming that 10–40 per cent of the accreted mass is launched into a jet, we find that in 10 yr a jet of no more than 0.2–$1.2 \times 10^{-2}\,M_\odot$ could be launched, a range that still overlaps with the lower range of the estimates of Soker & Kashi (2012). However, the Eddington luminosity calculation assumes spherical accretion. The disc accretion considered here allows greater accretion rates (e.g. Krumholz et al. 2009; Shiber, Schreier & Soker 2015), something that we discuss further in Section 5.3.

Next, we determine the magnetic field needed to launch the jets to check its consistency with the calculations above. We assume that the jet is launched by a magnetic field threading the disc. To constrain the magnetic field strength, we assume equipartition between the gas pressure in the disc and the magnetic pressure, $P_m = B^2/8\pi$. The gas pressure close to the companion is shown in Fig. 11. This pressure value must be a lower limit because our grid resolution is an order of magnitude too large to resolve the inner part of the disc. Therefore, we find that close to the companion the gas pressure is $>10^{4.3}$ Ba and that the magnetic field must therefore be >700 G.

Wardle (2007) and Tocknell, De Marco & Wardle (2014) estimated the magnetic field in an accreting disc using a formalism designed originally for accretion discs around forming stars. They assumed that the magnetic field responsible for the jet also produces the viscosity that leads to angular momentum loss and accretion (if another form of viscosity were to be present this would overestimate the magnetic field strength). We note that this expression is *local* to a given disc radius and does not attempt to describe how the magnetic field strength redistributes in response to accretion. We also note that this expression is for a geometrically thin disc. However, the difference for a thicker disc would be of the order of a factor of $\sqrt{r/H}$ (where H is the pressure scaleheight), which for us is only a factor of 1.2, even neglecting the effect of disc cooling, which will lead to a thinner disc.

Following Wardle (2007) and using as the local accretion rate $\dot{M} = 0.003\,M_\odot\,\mathrm{yr}^{-1}$ at radius $r = 1.5\,R_\odot$, the poloidal magnetic field at that location can be found to be:

$$B_p \approx (19\,\mathrm{kG}) \left(\frac{\dot{M}}{0.003\,M_\odot\,\mathrm{yr}^{-1}} \right)^{1/2}$$

$$\times \left(\frac{r}{1.5\,R_\odot} \right)^{-5/4} \left(\frac{M}{1.7\,M_\odot} \right)^{1/4}. \tag{5}$$

With this poloidal field, the toroidal component will be a factor of several larger, depending on the value assumed for the viscous α parameter (Shakura & Sunyaev 1973; Blackman, Frank & Welch 2001).

The radial dependence of the gas pressure in the disc is well matched by a power law: $P \propto r^{-2}$ for distances from the companion larger than $\sim73\,R_\odot$, corresponding to the 3 cell smoothing length. Extrapolating this power law to $1.5\,R_\odot$ from the companion, we find that the pressure there would be $\sim3.5 \times 10^7$ Ba, equal to the magnetic pressure of a $30\,\mathrm{kG}$ magnetic field. This value is in order-of-magnitude agreement with the magnetic field strength value inferred using the viscosity argument of Wardle (2007).

Since a lower companion mass requires a shorter orbit in order for significant mass transfer to take place and a massive disc to form around the companion, the accretion rate must be even larger than we considered above in order to accrete the whole disc before the next periastron passage and the following CE interaction. A larger companion mass, on the other hand, can cause greater mass transfer even with a larger periastron separation. In this case then, a longer orbit following the first periastron passage is possible and it might be more likely that the whole disc accretes before the next periastron passage occurs. We also found the most massive disc in our simulations in simulation no. 8, so a more massive companion appears most likely to lead to a massive jet.

5 DISCUSSION

5.1 Orbital stability after RLOF

A substantial disc forms in our simulation with mass ratio $q = 0.55$ only for $R < 2.5R_{\mathrm{star}}$ or 5.5 au. Larger values of q allow for larger separations, while smaller values of q require smaller separations. For a $3.05\,M_\odot$ AGB star the maximum AGB radius during thermal pulses is between 2.6 and 3.3 au (Madappatt, De Marco & Villaver 2015). Hence the periastron distance at which RLOF takes place could be as far as 8 au. For an interaction to happen at periastron passage, orbital periods cannot exceed a couple of decades or else the eccentricity would be unrealistically large. In addition, if a sufficiently massive disc is to be formed the orbit is shortened and the time to the inevitable CE becomes very short indeed (2–3 orbital periods).

For separations of $R \simeq 2.5R_{\mathrm{AGB}}$ (and $q = 0.55$), a less massive disc is formed but during the next periastron passage the situation becomes, again, that described above, and a sufficiently strong interaction forms a disc of a few hundredths of solar mass, after which a CE is inevitable. For larger periastron separations of $R \gtrsim R_{\mathrm{AGB}}$, a RLOF disc does not form (although a much less massive disc can form from accretion of wind material; Huarte-Espinosa et al. 2013) and the orbit is stable over tidal time-scales.

5.2 The post-CE separation and unbound mass

In the present simulations, at most 10 per cent of the AGB star's envelope mass has been unbound during the CE interaction. The

final separations of the CE cores range between 0.2 and 0.6 au (Table 1). If the final separation were affected by the limited resolution, the final separations in our simulations would be upper limits and the unbound masses would be lower limits.

The question of what the post-CE separation should be remains wide open. Simulations tend to predict larger, post-dynamical phase separations compared to observations (e.g. Passy et al. 2012), but the phase immediately following the post-dynamical phase (phases III and IV in Ivanova et al. 2013) could alter that separation further by any of a number of mechanisms. In-fall of bound material would reduce the separation further. On the other hand, the action of energy sources unaccounted for in current simulations could help eject the envelope contributing to larger separations (e.g. Nandez et al. 2015). In summary, we leave the question of the final separations unanswered, including the issue of whether a system like this could ever merge (see also Section 5.4). However, if a merger does not occur, the final separation will be small, much less than 1 au. For the case of the Rotten Egg Nebula the binary must have merged because the primary is still an AGB star with an envelope.

5.3 Disc and jets

The main goal of this study was to determine how massive a disc would be formed via RLOF at periastron passage. The accretion discs in our simulations have masses of a few hundredths of a solar mass and last on the order of a decade. The peak mass accretion rate into the disc is 0.01 $M_{\odot}$ yr^{-1}. This mass is distributed in a slightly flattened, rotating structure with a large scale-height of $\sim 0.7\,r$. The orbital period is half a year at $\sim 64\,R_{\odot}$. How this disc changes over the decade after formation and before more mass is added to it or a CE destroys it, depends on the magnetic field and on the radiative properties of the gas.

The peak accretion rate on to the disc, 0.01 $M_{\odot}$ yr^{-1} would be sufficient to create a jet of the needed mass over the available time only if that accretion rate were maintained across the disc radius and on to the companion. This accretion rate would be super-Eddington. Limiting ourselves to the Eddington accretion of 0.002–0.003 $M_{\odot}$ yr^{-1}, could generate jets with a mass of only 0.2–1.2 $\times$ $10^{-2}\,M_{\odot}$, which is at the lower end of the range of 1–2 $\times$ 10$^{-2}\,M_{\odot}$ discussed by Soker & Kashi (2012). The momentum of our highest mass jet would also be too low since its velocity could only be as high as 655 km s^{-1}, short of the needed 1000 km s^{-1}.

This said, our jets are not much less massive, or less energetic than required by the observations and the error bar both in the observations and in our simulations may bring the values into agreement. Additionally, there are other possibilities that would boost the predicted jet mass: the jet launch efficiency could be higher and/or additional gas ejected following the second periastron passage, when the simulations show that there is a brief period of ~ 4–5 yr before the third periastron passage leads to the CE. Another, more likely possibility is that the accretion is super-Eddington. The Eddington limit applies to spherical accretion and assumes that all the generated energy goes into radiation. Neither of these assumptions likely applies in our situation, in which the accretion is likely equatorial and much of the energy goes into kinetic energy of the jets.

Finally we point out that if the companion had been a WD, escape speeds (and hence jet speeds) as high as 1000 km s^{-1} would easily have been achieved. However, the mass accretion rates would be lower than for a main-sequence star, once the combination of plausible masses and overall lower accretion radii are combined with the Eddington limit reasoning above. A typical white dwarf will have a mass of $\sim 0.6\,M_{\odot}$ as in simulation no. 7, where we

found that because of the companion's lower mass, the periastron separation must be smaller in order to achieve significant mass transfer, which means that the orbital period will be shorter. Hence, there would be very little time available to launch a jet, necessitating very high accretion rates in order to produce jets like those observed in the Rotten Egg Nebula.

A more massive main-sequence companion (simulation no. 8) can also allow for higher ejection speeds, as the escape speed from main-sequence stars increases with mass. However, since the companion cannot be much more massive than 3 $M_{\odot}$, this can only increase the escape speed from the object by ~ 15–20 per cent. A more massive companion does allow for a more massive disc and a longer period following the first periastron passage, allowing for more mass to be launched into a jet, but a merger is less likely (De Marco et al. 2011).

5.4 The status of the Rotten Egg Nebula

The central star in the Rotten Egg Nebula is observed to be a binary containing an AGB star and a main-sequence companion at a separation larger than 10 au (Sánchez Contreras et al. 2004). The nebula includes a relatively massive circumbinary torus and collimated lobes. In this paper, we have scrutinized the proposal (Soker & Kashi 2012) that the nebula formed ~ 800 yr ago, during a periastron passage of the binary, by the mechanism of RLOF and jet formation.

To do so, we have performed a number of grid-based hydrodynamic simulations of the interaction of a 3.05 $M_{\odot}$ AGB star and a less massive companion in an eccentric orbit, with a range of eccentricities, initial periastron separations and companion masses. We have found that for periastron separations greater than $\sim 2.5\,R_{\mathrm{AGB}}$ ≈ 5.5 au, there is no significant mass transfer until tidal forces bring the companions closer together on tidal time-scales. To restrict the range of periastron separations to be smaller than this limit, the orbit cannot have a period of the order of 800 yr, unless the eccentricity is almost unity. Adopting more reasonable eccentricity values the longest periods that still maintain a periastron distance small enough for RLOF are of the order of a few decades.

Such a range of periods would mean that, for the detected A0V companion to be responsible for the 800 yr old nebula, not all periastron passages result in an interaction. This could be explained if an interaction only took place during the last thermal pulse of the Mira (lasting ~ 100 yr), ~ 800 yr ago. Today, the companion would be back to a smaller, interpulse radius and not interacting.

However, we also found that if significant mass transfer occurs, the orbit is altered in such a way that within a couple more orbits the system enters a CE interaction. The result of the CE interaction can be either a merger, or an AGB star that then evolves in isolation, or a post-AGB star orbited by a companion with a period of ~ 1 d (Ivanova et al. 2013). Since the central star of the Rotten Egg Nebula is an AGB star, then the companion must have merged and we are forced to conclude that if an eccentric binary produced this nebula, then the system must have initially been a triple: a close companion to the AGB star has merged with it, producing the nebula, while the more distant A-type companion remains. In such case, the A-star would be a by-stander. For such a triple system to be stable, the A-type companion must be farther than 10 au, in line with the observations.

In our scenario, the AGB star is the pre-interaction primary. Since we have no constraints on the mass of the AGB star today, we cannot tell what the mass of the companion that merged with it was, except that it must have been less massive than the progenitor mass of

the AGB star. Hence, the current AGB star should be in the range $3\,M_\odot < M_{AGB} < 6.5\,M_\odot$. We do not know what consequences this merger may have had on the AGB star, but as the merger would have occurred ~800 yr ago, it is unlikely that the AGB star would have had time to evolve away from the AGB and it should therefore still be seen as an AGB star.

We also found that the disc-like structure of material dragged off the AGB star during the periastron passage of the companion that eventually merged, could be responsible for lobes with the observed characteristics for plausible parameters of the magnetic field structure and by allowing for a super-Eddington accretion rate on to the companion (Shiber et al. 2015).

This said we should not ignore that every phase of the evolution of a system like ours, both before and during the CE phase is riddled with uncertainties (for a review see Ivanova et al. 2013). The tidal interaction (pre-CE) phase may include enhanced, companion-induced mass-loss (Tout & Eggleton 1988), which may result in a lighter envelope at the time of CE. The eccentricity, which should be rapidly reduced by tides, may actually be pumped to higher values by mass-loss, resulting in a system that will interact in the way we simulate (Soker 2000). As for whether a CE would result after RLOF, our simulated system, with the mass ratio of $M_d/M_a = 1.79$ should be prone to unstable mass transfer and CE (Podsiadlowski 2001), although the seldom considered case of eccentric orbits might alter the predictions. Finally, whether a system like ours could merge inside the CE is not clear either: while there is enough orbital energy to unbind the envelope, this criterion alone is not sufficient to determine the outcome of the CE and depends sensitively on the efficiency of the interaction (De Marco et al. 2011; Passy et al. 2012; Ivanova et al. 2013). It is possible that a lower mass companion may be needed to achieve a merger inside the primary's CE, but lower mass discs typically formed around a lower mass companion would have more difficulty in achieving the needed jet energies and momenta.

An eccentric binary has been proposed to explain other objects similar to The Rotten Egg Nebula, such as IRAS22036+5306 (Sahai et al. 2006; Soker & Kashi 2012), or planetary nebulae with certain distinctive features (Soker & Hadar 2002). We therefore think it is worth pursuing the current line of investigation in the context of other observed objects, using a range of additional input parameters and with more highly resolved simulations, which would lower some of the uncertainties.

6 SUMMARY

We have performed a number of grid-based 3D hydrodynamic simulations of eccentric binaries consisting of an AGB star and a less massive main-sequence companion. We found that:

(i) In order for significant mass ($\gtrsim 0.01\,M_\odot$) to be transferred to the companion, the periastron passage must be $\lesssim 2.5 R_{star} \approx 5.5$ au in our setup. If significant mass transfer occurs, the orbit is altered in such a way that a CE interaction event ensues after a few more orbits, which will either eject the envelope and lead to a short-period binary, or lead to a merger that retains the envelope.

(ii) We found that little mass is unbound in the CE interaction, $\lesssim 0.4\,M_\odot$ in all of our simulations. Most of the envelope therefore remains bound.

(iii) Following periastron passage, but before the CE interaction begins, an intermediate phase occurs where the companion is surrounded by a disc-like structure that with a suitable magnetic

field can launch jets. Such a field appears likely if equipartition is assumed.

(iv) Provided accretion rates larger than the spherical Eddington limit and reasonable jet launching efficiency, the lobes in the Rotten Egg Nebula could be formed this way. However, since that object now consists of an AGB star and a main-sequence companion, and we have concluded that the interaction leads to a merger, we suggest that if the nebula was formed through RLOF in an eccentric binary, the system must initially have been a triple where two objects merged to form today's AGB star.

The next step in the study of this system and systems like it, is the use of adaptive mesh refinement and the relaxation of the adiabatic approximation. Simulating a triple system would incur many additional challenges, including the need to simulate larger volumes and to run the simulation for a longer physical time.

REFERENCES

Alcolea J., Bujarrabal V., Sánchez Contreras C., Neri R., Zweigle J., 2001, A&A, 373, 932
Blackman E. G., Frank A., Welch C., 2001, ApJ, 546, 288
Bryan G. et al., 2014, ApJS, 211, 19
Bujarrabal V., Alcolea J., Sánchez Contreras C., Sahai R., 2002, A&A, 389, 271
Cantiello M., Mankovich C., Bildsten L., Christensen-Dalsgaard J., Paxton B., 2014, ApJ, 788, 93
Church R. P., Dischler J., Davies M. B., Tout C. A., Adams T., Beer M. E., 2009, MNRAS, 395, 1127
De Marco O., Passy J.-C., Moe M., Herwig F., Mac Low M.-M., Paxton B., 2011, MNRAS, 411, 2277
Desmurs J.-F., 2012, IAU Symp., 287, 217
Eggleton P. P., 1983, ApJ, 268, 368
Federrath C., Schrön M., Banerjee R., Klessen R. S., 2014, ApJ, 790, 128
Huarte-Espinosa M., Carroll-Nellenback J., Nordhaus J., Frank A., Blackman E. G., 2013, MNRAS, 433, 295
Ireland M. J., Scholz M., Wood P. R., 2011, MNRAS, 418, 114
Ivanova N., Chaichenets S., 2011, ApJ, 731, 36
Ivanova N. et al., 2013, A&AR, 21, 59
Ivanova N., Justham S., Podsiadlowski P., 2015, MNRAS, 447, 2181
Jiang Y.-F., Belyaev M., Goodman J., Stone J. M., 2013, New Astron., 19, 48
Jura M., Morris M., 1985, ApJ, 292, 487

Kashi A., Soker N., 2010, preprint (arXiv:1011.1222)
Kashi A., Frankowski A., Soker N., 2010, ApJ, 709, 11
Krumholz M. R., Klein R. I., McKee C. F., Offner S. S. R., Cunningham A. J., 2009, Science, 323, 754
Lajoie C. P., Sills A., 2011, ApJ, 726, 67
Madappatt N., De Marco O., Villaver E., 2015, MNRAS, submitted
Mermilliod J. C., 1981, A&A, 97, 235
Nandez J. L. A., Ivanova N., Lombardi J. C., 2015, MNRAS, 450, 39
Nicholls C. P., Wood P. R., 2012, MNRAS, 421, 2616
O'Shea B. W., Bryan G., Bordner J., Norman M. L., Abel T., Harkness R., Kritsuk A., 2004, preprint (astro-ph/0403044)
Passy J.-C. et al., 2012, ApJ, 744, 52
Paxton B., Bildsten L., Dotter A., Herwig F., Lesaffre P., Timmes F., 2011, ApJS, 192, 3
Paxton B. et al., 2013, ApJS, 208, 4
Podsiadlowski P., 2001, ASP Conf., 229, 239
Pudritz R. E., Hardcastle M. J., Gabuzda D. C., 2012, Spave Sci. Rev., 169, 27
Rasio F. A., Livio M., 1996, ApJ, 471, 366
Ricker P. M., Taam R. E., 2012, ApJ, 746, 74
Sahai R., Young K., Patel N. A., Sánchez Contreras C., Morris M., 2006, ApJ, 653, 1241

Sánchez Contreras C., Gil De Paz A., Sahai R., 2004, ApJ, 616, 519
Sandquist E. L., Taam R. E., Chen X., Bodenheimer P., Burkert A., 1998, ApJ, 500, 909
Schwarz H. E., Nyman L.-A., Seaquist E. R., Ivison R. J., 1995, A&A, 303, 833
Sepinsky J. F., Willems B., Kalogera V., 2007, ApJ, 660, 1624
Shakura N. I., Sunyaev R. A., 1973, A&A, 24, 337
Shiber S., Schreier R., Soker N., 2015, preprint (arXiv:1504.04144)
Soker N., 2000, A&A, 357, 557
Soker N., Hadar R., 2002, MNRAS, 331, 731
Soker N., Kashi A., 2012, ApJ, 746, 100
Staff J. E., Koning N., Ouyed R., Thompson A., Pudritz R. E., 2015, MNRAS, 446, 3975
Tocknell J., De Marco O., Wardle M., 2014, MNRAS, 439, 249
Tout C. A., Eggleton P. P., 1988, MNRAS, 231, 823
Wardle M., 2007, Ap&SS 311, 35
Zanni C., Ferreira J., 2013, A&A, 550, 99

This paper has been typeset from a TEX/LATEX file prepared by the author.